COMMUNICATION

Check for updates

Porous carbon nitride fullerenes: a novel family of porous cage molecules†

Zacharias G. Fthenakis and Nektarios N. Lathiotakis

A novel family of cage molecules, porous carbon nitride fullerenes (PCNFs), is designed, proposed and studied theoretically. PCNFs can be considered the zero-dimensional counterparts of two-dimensional porous graphitic carbon nitrides, in analogy with icosahedral fullerenes, being the zero-dimensional counterparts of graphene. The study is focused on two representative members of the PCNF family: icosahedral $C_{60}N_{60}$ and $C_{120}N_{60}$, which are the first members of the two main subfamilies of these structures. Given the advanced potential of two-dimensional graphitic carbon nitrides for several interesting applications, it is reasonable to expect that this potential extends to their zero-dimensional counterparts. The present study demonstrates the electronic, vibrational, and thermal stability of the two representative PCNFs utilizing density functional theory and molecular dynamics simulations with ReaxFF potentials. In addition, their structural, vibrational, and electronic properties are revealed.

New concepts

Molecular design plays a vital role in the development of new molecules with novel and interesting properties, and the potential to be used in several applications, which may range from catalysis and molecular trapping to the discovery of new drugs or biomolecules. Considering the relationship between a honeycomb lattice (graphene) and Goldberg polyhedra (icosahedral fullerenes), and the structural transformations that turn a honeycomb lattice (graphene) into the geometrical structure of graphitic porous carbon nitrides, a novel family of porous cage molecules with N-terminated pores, porous carbon nitride fullerenes (PCNFs), is designed and proposed. PCNFs are the zero-dimensional (0D) counterparts of two-dimensional (2D) graphitic carbon nitrides, just as icosahedral fullerenes are the 0D counterparts of graphene. This theoretical study demonstrates their dynamic, electronic, and thermal stability, as well as their unique geometrical features. Inheriting the interesting properties of 2D graphitic carbon nitrides and having these unique geometrical features, PCNFs could be ideal structures for potentially interesting applications, such as permeation, molecular trapping, catalysis, *etc.*, beyond those of their 2D counterparts. Therefore, PCNFs have the potential to become a promising novel class of fullerene-based cage molecules opening up new avenues in nanomaterials research and technology.

1. Introduction

Given that fullerenes are the zero-dimensional (0D) analogues of graphene, a question that naturally arises is whether 0D fullerene analogues of two-dimensional (2D) porous graphitic carbon nitrides (g-C_nN_m) exist.

Porous g-C_nN_m constitute a family of periodic graphene-based structures, incorporating substitutional N atoms in several sites of a porous graphene lattice. N atoms in these structures can be pyridinic (at the pore edges) and maybe graphitic, substituting 2- and 3-fold coordinated C atoms, respectively. Several g-C_nN_m have been reportedly synthesized.[1–9] Two structures that have attracted considerable attention are g-CN[8,9] and g-C_2N,[4–8] exhibiting a broad spectrum of applications, which include catalysis[2,10–19] (such as photocatalytic water splitting[2,16–18] and single atom catalysis[19]), gas separation[20–26] and nanofiltration,[27] water desalination,[28] hydrogen storage,[29] and anode materials for Li-ion batteries.[30] Given that porous g-C_nN_m and their 0D counterparts would be structurally very similar, it is reasonable to expect that the former's intriguing properties would be inherited by the latter which may exhibit additional novel properties due to their specific cage geometry and finite size. Hence, the elevated interest in them is more than obvious.

Considering that (i) the relationship between these 0D fullerene-like structures and porous g-C_nN_m is analogous to the connection between icosahedral fullerenes and graphene, and (ii) the design of porous g-C_nN_m involves the formation of pores and substitution of appropriate C atoms with N atoms, as described above, the form of these molecules can be easily derived from Goldberg polyhedra,[31] in a similar way to the

[a] Istituto Nanoscienze, Consiglio Nazionale delle Ricerche (CNR), and National Enterprise for nanoScience and nanoTechnology (NEST), Scuola Normale Superiore, 56127 Pisa, Italy. E-mail: zacharias.fthenakis@nano.cnr.it

[b] Theoretical and Physical Chemistry Institute, National Hellenic Research Foundation, GR-11635, Athens, Greece. E-mail: fthenak@eie.gr, lathiot@eie.gr

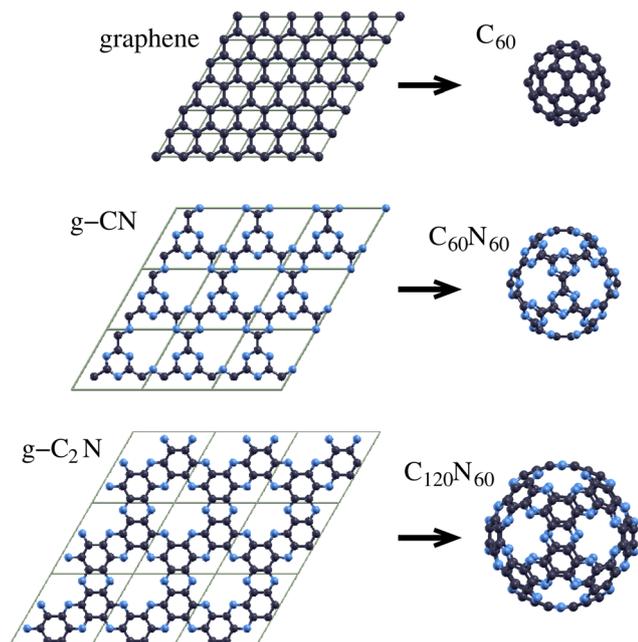† Electronic supplementary information (ESI) available. See DOI: https://doi.org/10.1039/d5nh00091b

Fig. 1 2D structures (graphene and g-C_nN_m) and their fullerene counterparts.
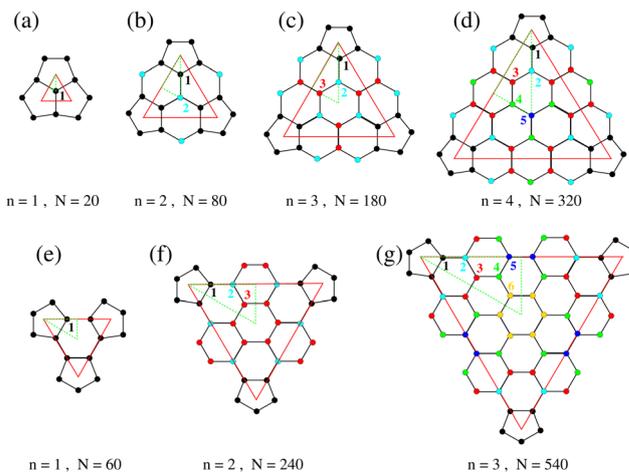

Fig. 2 Icosahedrally repeated building blocks (red triangles) for the construction of the first members of the $(n, 0)$ (panels (a)–(d)) and (n, n) (panels (e)–(g)) Goldberg polyhedra. The red triangles represent the triangular faces of an icosahedron connecting the centers of neighboring pentagons. The green dashed-line triangles represent the irreducible part of each such triangular face. Equivalent vertices (atoms) are shown with the same color and the vertices of the irreducible part are numbered.

design of icosahedral fullerenes. The design of such 0D structures, which we call "*porous carbon nitride fullerenes*" (PCNFs), involves the formation of proper pores in icosahedral fullerenes in a way that retains full icosahedral symmetry. The design process is discussed in the next section. As we show, the smallest members of icosahedral fullerenes that can be the precursors of PCNF design are C_{180} and C_{240}. The PCNFs derived from them are $C_{60}N_{60}$ and $C_{120}N_{60}$, respectively, corresponding to the g-CN and g-C_2N 2D structures. These PCNFs ($C_{60}N_{60}$ and $C_{120}N_{60}$) together with the corresponding 2D structures (g-CN and g-C_2N, respectively) are shown in Fig. 1. In the same figure, graphene and icosahedral C_{60} are also shown, to emphasize the relationship between (i) graphene and C_{60}, (ii) graphene and g-C_nN_m, and (iii) icosahedral fullerenes and PCNFs. In the present work, we theoretically study $C_{60}N_{60}$ and $C_{120}N_{60}$ as representatives of the PCNF family as well as C_{60} for comparison. Our results demonstrate the capability of this family of structures to open up new directions in nanomaterials research and technology and become the new generation of fullerene-based cage molecules.

2. Theoretical design of PCNFs

Fullerenes with rotational icosahedral symmetry are topologically equivalent to the Goldberg polyhedra,[31] which contain only pentagons and hexagons. In particular, they contain exactly 12 pentagons on the vertices of an icosahedron, with its 20 equilateral triangular faces composed of hexagons in a honeycomb lattice arrangement. Each such triangular face (and in turn, the polyhedron itself) is characterized by two integer numbers (n, m), defining the lattice vector $n\boldsymbol{a} + m\boldsymbol{b}$ of

the honeycomb lattice, which represents one of the three edges of that triangle, with $\boldsymbol{a}$ and $\boldsymbol{b}$ being the primitive lattice vectors of the honeycomb lattice.

There are three classes of Goldberg polyhedra, namely $(n, 0)$, (n, n), and (n, m) with $n \neq m$. The triangular faces of the icosahedra corresponding to the first members of the $(n, 0)$ and (n, n) classes are shown schematically in Fig. 2 with red lines. Class $(n, 0)$ and (n, n) polyhedra (fullerenes) have full icosahedral symmetry[32] (*i.e.* apart from the rotational icosahedral symmetry, they also have mirror symmetry), and they contain $N = 20 \, n^2$ and $N = 60 \, n^2$ vertices (atoms), respectively. For the Goldberg polyhedra corresponding to the triangles shown in Fig. 2, the numbers n and N are shown below each triangle. Panels (a)–(d) represent the triangles for the first $(n, 0)$ polyhedra and panels (e)–(g) for the first (n, n) polyhedra.

Due to symmetry reasons, there is an irreducible part of each such triangle corresponding to the 1/6th of it. This irreducible part is a right triangle, shown for each case in the same figure by a green dashed line. Thus, as far as the icosahedral symmetry is retained, only the atoms in that irreducible part may behave independently, while all other atoms have an equivalent one in the irreducible part. In all cases shown in Fig. 2, the atoms in the irreducible part are numbered from 1 to 6. The atom numbered "1" (black) is the one in the pentagonal rings. The design of a fully icosahedral PCNF implies the introduction of pores into the corresponding fullerene by removing C atoms from the irreducible part of the "triangular faces" and all the equivalent C atoms in that fullerene. Then two-fold C atoms at the pore boundaries are replaced by pyridinic N atoms, and maybe some three-fold coordinated C atoms by graphitic N atoms. We should note that the above process is only for conceptualization and does not constitute a synthetic route.

The design procedure we described cannot be applied to C_{20} and C_{60}, since the irreducible part of their "triangular faces" contains only one atom (see Fig. 2(a) and (e), respectively). Thus, removing that atom and its equivalents would eliminate the entire fullerene. This design procedure is also not applicable to C_{80}. The corresponding "triangular face" of C_{80} has two atoms in its irreducible part (see Fig. 2(b), where these atoms are numbered "1" and "2"). If atom 1 and its equivalents are removed, atom 2 and its equivalents are left disconnected. Removing atom 2 and its equivalents results in disconnected pentagons formed by atom 1 and its equivalents. Consequently, none of the C_{20}, C_{60} and C_{80} can be used as precursors for the formation of PCNFs. On the other hand, the next members of $(n, 0)$ and (n, n) fullerenes, C_{180} and C_{240}, respectively, can be used as precursors for the formation of the $C_{60}N_{60}$ and $C_{120}N_{60}$ PCNFs, respectively, which are studied in the present work. They are both derived by removing all pentagonal rings of C_{180} and C_{240} fullerenes, represented by atom 1 and its equivalents in Fig. 2(c) and (f), respectively. $C_{60}N_{60}$ and $C_{120}N_{60}$ are the only PCNF structures that can be derived from C_{180} and C_{240}, respectively, while more than one PCNF can be derived from the next $(n, 0)$ and (n, n) icosahedral fullerenes (e.g. the C_{320} and C_{540}, respectively, and all the higher members of these fullerene subfamilies). For these fullerenes, several other options exist for removing C atoms to design PCNFs, apart from removing all pentagons, which is always an option for them.

3. Equilibrium structures – structural and vibrational properties

As already mentioned, in the present study we focus on $C_{60}N_{60}$ and $C_{120}N_{60}$ as representatives of the whole family of PCNFs. For the structural and vibrational properties, we employ density functional theory (DFT) with the state-of-the-art, range-separated, hybrid ωB97X-D[33] and hybrid meta-GGA MN15[34] functionals, as implemented in the Gaussian 16 code,[35] with the 6-311G(d,p) basis set.

The equilibrium structures for $C_{60}N_{60}$ and $C_{120}N_{60}$ are shown in Fig. 3 from two different perspectives. Their geometries obtained using the ωB97X-D and MN15 functionals are practically identical. The Cartesian coordinates of the optimal geometries are included in the ESI† (in xyz format). As we can see, they are composed of C_3N_3 and C_4N_2 hexagons, respectively, interconnected by C–C bonds. In $C_{120}N_{60}$, these interconnecting bonds and the C–C bonds within C_4N_2 hexagons form hexagonal carbon rings. Vibrational analysis shows that all eigenvalues of the dynamical matrix are positive (real vibrational frequencies), indicating dynamic stability. The minimum frequencies, ν_{min}, obtained are shown in Table 1.

Fig. 1 shows that these structural features of $C_{60}N_{60}$ and $C_{120}N_{60}$, and their stoichiometry, are identical to those of g-CN and g-C_2N, respectively. Their main morphological differences are their curvature and the pentagonal form of the pores (33333 in the Fthenakis nomenclature[36,37]) instead of the planarity and the hexagonal pores (333333)[38] of g-CN and
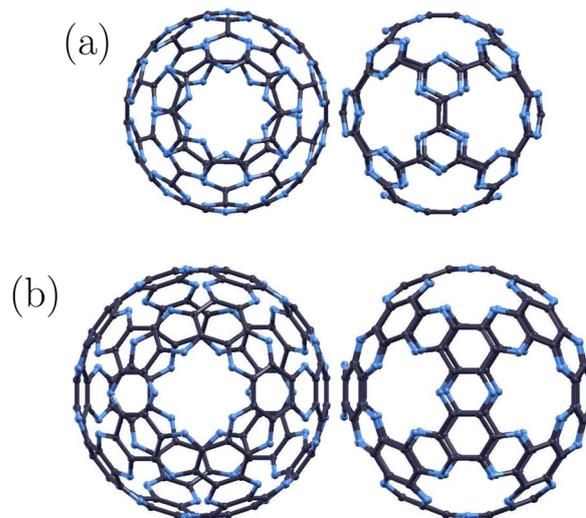

Fig. 3 Structures of (a) $C_{60}N_{60}$ and (b) $C_{120}N_{60}$ from two different viewpoints. C atoms are shown in black and N atoms in blue.

Table 1 Structural, electronic and vibrational features of $C_{60}N_{60}$ and $C_{120}N_{60}$ calculated utilizing the ωB97X-D and MN15 functionals. All interatomic distances, energies, charges, and minimum frequencies (ν_{min}) are given in Å, eV, electrons, and cm^{-1}, respectively

Funct.	$C_{60}N_{60}$		$C_{120}N_{60}$		C_{60}	
	ωB97X-D	MN15	ωB97X-D	MN15	ωB97X-D	MN15
d_{C-C}, d_{hp}	1.520	1.518	1.478	1.477	1.448	1.448
d_{C-C}, d_{hh}			1.413	1.417	1.383	1.387
d_{C-N}	1.327	1.330	1.325	1.328		
δd	0.023	0.023	0.066	0.065		
D	4.553	4.561	4.561	4.573		
d_{C-C}^{sphere}	11.314	11.332	13.314	13.321	7.059	7.070
d_{N-N}^{sphere}	11.392	11.410	13.461	13.465		
IP	9.20	9.23	8.56	8.08	8.56	8.01
EA	2.08	2.60	2.19	2.79	2.32	2.45
η	3.56	3.32	3.18	2.64	2.84	2.67
HOMO	−9.73	−8.68	−8.65	−7.61		
LUMO	−2.02	−3.15	−2.23	−3.28		
Δ_{H-L}	7.71	5.53	6.42	4.32	6.00	3.92
Mulliken population						
C atoms	0.24	0.20	0.12	0.095		
N atoms	−0.24	−0.20	−0.24	−0.19		
ν_{min}	75.6	76.1	90.0	88.2	270	263

g-C_2N. Unlike the C_{180} and C_{240} precursors, which contain pentagons and hexagons, $C_{60}N_{60}$ and $C_{120}N_{60}$ consist exclusively of hexagons.

Table 1 shows several structural properties of the two PCNFs (and C_{60}). As we can see, the C–N bonds for both PCNFs have the same length, $d_{C-N} \approx 1.33$ Å. On the other hand, two kinds of C–C bonds were found for $C_{120}N_{60}$: those interconnecting the C_4N_2 hexagons with length $d_{C-C} \approx 1.48$ Å, and those interconnecting the C_4N_2 hexagons with length $d'_{C-C} \approx 1.415$ Å, which differ from the C–C bond lengths of $C_{60}N_{60}$ ($d_{C-C} \approx 1.52$ Å). For C_{60}, the length of the common bonds of adjacent pentagons and hexagons (single bonds) is $d_{hp} \approx 1.45$ Å (d_{C-C} in Table 1), and the length of the common bonds of adjacent

hexagons (double bonds) is $d_{hh} \approx 1.39$ Å (d'_{C-C} in Table 1). These values are comparable to the d_{C-C} and d'_{C-C} bond lengths of $C_{60}N_{60}$ and $C_{120}N_{60}$, with $d^{C_{60}N_{60}}_{C-C} > d^{C_{120}N_{60}}_{C-C} > d_{hp}$ and $d'^{C_{120}N_{60}}_{C-C} > d_{hh}$. This is a strong indication that the C–C bonds of $C_{60}N_{60}$ and $C_{120}N_{60}$ with lengths d_{C-C} and d'_{C-C} exhibit single and double bond characters, respectively, with the C–C bonds of $C_{60}N_{60}$ and $C_{120}N_{60}$ being weaker than those of C_{60}, and those of $C_{120}N_{60}$ being stronger than those of $C_{60}N_{60}$. The C_3N_3 hexagons of $C_{60}N_{60}$ and the C_4N_2 hexagons of $C_{120}N_{60}$ are almost planar, with only a small outward elevation δd of the N atoms, with respect to the C atom plane ($\delta d = 0.023$ Å and 0.066 Å, respectively).

The diameter of the pores, defined as the diameter of the N-atom pentagon's circumscribed circle, is $D \approx 4.56$ Å for both structures. Since the diameter D and the atomic environment of the pores for both $C_{60}N_{60}$ and $C_{120}N_{60}$ are practically the same, the molecular permeation properties of those pores are also expected to be similar. The local curvature is the only parameter that may differentiate these properties, varying between the two PCNFs. It is worth noting that the pore diameter falls within the range of interest for the permeation of small molecules.[20–22,24,26,38] To the best of our knowledge, these pentagonal pores have not been observed in other structures and their properties make PCNFs particularly interesting.

The diameters of the two PCNFs, defined as the distance between diametrically opposite C or N atoms (d^{sphere}_{C-C} and d^{sphere}_{N-N}, respectively), are ≈ 11.3 and 11.4 Å for $C_{60}N_{60}$ and ≈ 13.3 and 13.5 Å for $C_{120}N_{60}$, i.e. the diameter of $C_{120}N_{60}$ is approximately 2 Å larger than that of $C_{60}N_{60}$, and almost twice as large as that of C_{60}. Given the size of the PCNFs, they may hold promise as traps for small molecules or metal clusters. Molecule trapping in these systems has the potential for a wide range of applications.

4. Electronic properties

We calculate the electronic properties using the same DFT method as the one used for calculating the structural and vibrational properties of $C_{60}N_{60}$ and $C_{120}N_{60}$. Due to the icosahedral symmetry of $C_{60}N_{60}$ and $C_{120}N_{60}$, the energy levels are in most cases degenerate. In particular, the HOMOs for $C_{60}N_{60}$ and $C_{120}N_{60}$ are five- and three-fold degenerate, respectively, while the LUMOs are three- and five-fold degenerate, respectively. However, in both cases, the HOMOs are fully occupied, enhancing stability, like in the case of the aromatic ring molecules.

The electron densities corresponding to all five (for $C_{60}N_{60}$) and all three (for $C_{120}N_{60}$) degenerate HOMOs are shown in Fig. 4(a) and (b), respectively, providing information on the distribution of all electrons at the HOMO energy level. As we can see, they have entirely different characters. The HOMOs of $C_{60}N_{60}$ are dominated by nitrogen sp^2 lone-pair states with a minor contribution from the sp^2 carbon orbitals, while for $C_{120}N_{60}$, they have the character of $p_\perp$ orbitals. With $p_\perp$ we mean p-orbitals directed perpendicular to the $C_{120}N_{60}$ surface

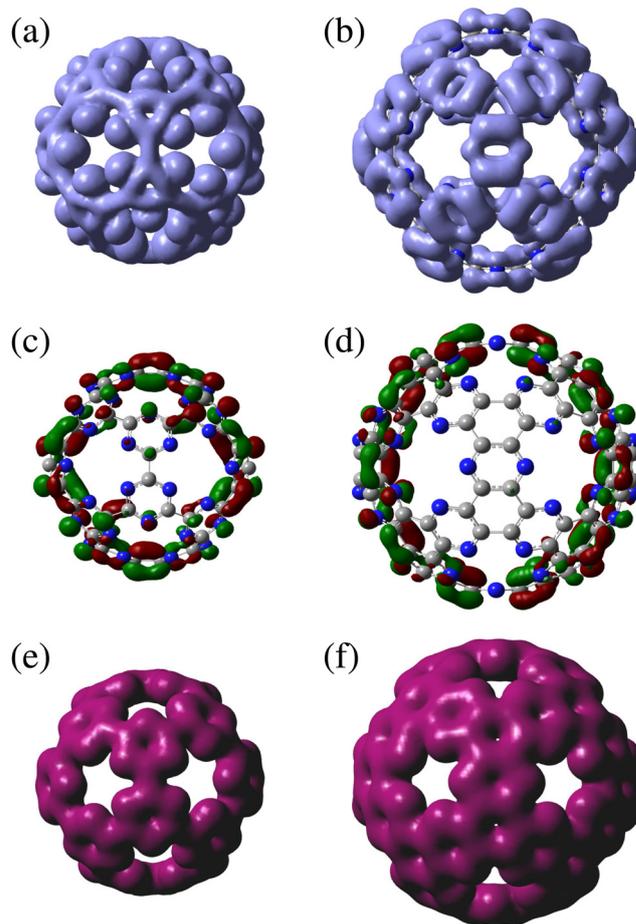Fig. 4 Electron density corresponding to all degenerate HOMOs of $C_{60}N_{60}$ (a) and $C_{120}N_{60}$ (b). One of the degenerate LUMOs of $C_{60}N_{60}$ (c) and $C_{120}N_{60}$ (d). Total electron density of $C_{60}N_{60}$ (e) and $C_{120}N_{60}$ (f).

locally. Moreover, one can see that the electron density of HOMOs for $C_{120}N_{60}$ is high along the C–C bonds of the C_4N_2 hexagons, indicating the presence of a double bond. Instead, along the C–C bonds interconnecting the C_4N_2 hexagons, it almost vanishes, in consistency with the presence of a single bond. These results support the discussion about the bond lengths in Section 3. It can also be seen from Fig. 4(b) that the $p_\perp$ contribution of N atoms is relatively small compared to that of the C atoms.

The LUMOs, on the other hand, are of $p_\perp$ orbital character for both structures, as shown in Fig. 4(c) and (d), where one of the degenerate LUMOs of $C_{60}N_{60}$ and $C_{120}N_{60}$ is shown, respectively. Although not shown, the other degenerate LUMOs have the same character differing in the location. We show the total electron density of $C_{60}N_{60}$ and $C_{120}N_{60}$ in Fig. 4(e) and (f).

Our findings on the nature of the HOMOs and LUMOs of $C_{60}N_{60}$ and $C_{120}N_{60}$ are very similar to that of the valence and conduction bands of g-CN[23] and g-C_2N,[18] respectively. For g-CN, the valence band consists of the sp^2 orbitals of the nitrogen atoms' lone-pair electrons, lying in the structure's plane and localized on the nitrogen atoms. Instead, the conduction band is composed of p_z orbitals of the C and N atoms.[23]

For g-C_2N, the valence band is composed mainly of the p_z orbitals of the C atoms, with a smaller contribution from the p_z orbitals of the N atoms. Instead, the conduction band is composed mainly of p_z orbitals of the N atoms.[18]

For both structures, there is a relatively large HOMO–LUMO gap (Δ_{H-L}) in comparison to the differences in the other successive energy levels, indicating a clear splitting of the π occupied states from the π^* unoccupied ones. The calculated HOMO, LUMO, and Δ_{H-L} values are shown in Table 1. It is worth noting that the values of HOMO/LUMO energy levels obtained using many popular DFT approximations are, in general, not accurate predictions of the spectral properties. However, it has been demonstrated that accuracy can be substantially improved by approximations like the non-empirically tuned range-separated functionals.[39–41]

The drop in the HOMO–LUMO gap from $C_{60}N_{60}$ to $C_{120}N_{60}$ seems to be similar to the behavior of the gap of graphene nanoribbons, which decreases as their width increases.[42] Furthermore, Mulliken population analysis reveals a weak charge transfer of ~ 0.2 electrons from each N atom to C atoms in both structures, which are equally distributed to the C atoms, while the total dipole moment of PCNFs is zero, due to their icosahedral symmetry.

4.1. Ionization potentials and electron affinities

With the same DFT method, the ionization potentials (IPs) and electron affinities (EAs) of $C_{60}N_{60}$ and $C_{120}N_{60}$ were also calculated as the absolute energy differences between the neutral molecule and positive and negative ions, respectively, with full geometry relaxation. The calculated IP and EA values, as well as the values of chemical hardness $\eta = (IP - EA)/2$, are shown in Table 1. The corresponding values for C_{60} are also presented in the same table, showing that (a) $\eta_{PCNFs} > \eta_{C60}$, which indicates that $C_{60}N_{60}$ and $C_{120}N_{60}$ are electronically more stable than C_{60}, and (b) $EA_{PCNFs} \approx EA_{C60}$, making PCNFs promising candidates as electron acceptors in several applications, like C_{60}. Notably, the absolute HOMO and LUMO values are relatively good measures of IPs and EAs for the state-of-the-art approximations chosen. The large Δ_{H-L} and η values strongly suggest that the electronic state of the studied PCNF structures is particularly stable.

4.2. Formation energies

The formation energies of $C_{60}N_{60}$ and $C_{120}N_{60}$ were calculated using periodic DFT calculations with the PBE functional, including D3 dispersion corrections of Grimme et al.,[43] as implemented in the Quantum Espresso code.[44] This methodology allows the treatment of the two molecules and their 2D counterparts at the same level of theory. We adopted the projector augmented wave method (and corresponding pseudopotentials) and kinetic energy cutoffs for the wavefunction and density of 60 and 500 Ryd, respectively. For the periodic structures, $24 \times 24 \times 1$ k-mesh was used, while for the two molecules, Γ-point calculations were performed in a cubic supercell of a 36 Å side.

The formation energy per atom, $\Delta E^{(f)}$, of $C_{60}N_{60}$, $C_{120}N_{60}$ and C_{60} with respect to their 2D counterparts g-CN, g-C_2N and graphene, respectively, is calculated as $\Delta E^{(f)} = E_{0D} - E_{2D}$, where E_{0D} and E_{2D} are the calculated total energies per atom of the 0D structures and their 2D counterparts. We found that the $\Delta E^{(f)}$ values for $C_{60}N_{60}$, $C_{120}N_{60}$ and C_{60} are 0.09, 0.08 and 0.38 eV per atom, respectively. The relatively large $\Delta E^{(f)}$ value for C_{60} can be explained in terms of the large bond length deviations of C_{60} from the bond length of graphene ($d = 1.42$ Å) and the corresponding relatively large bond angle deviations of the pentagonal angles (108°) from the hexagonal ones of graphene. The absence of pentagonal rings in $C_{60}N_{60}$ and $C_{120}N_{60}$ and the insignificant deviations of their bond lengths and angles from the corresponding ones of g-CN and g-C_2N, respectively, significantly reduce the additional energy to form the PCNFs, which is mainly attributed to the strain energy due to the curvature. This explains the relatively small $\Delta E^{(f)}$ values of $C_{60}N_{60}$ and $C_{120}N_{60}$.

For completeness, we also calculated the formation energies, $E^{(f)}$, of g-CN, g-C_2N, $C_{60}N_{60}$, $C_{120}N_{60}$, and Ih-C_{60} fullerene with respect to graphene and N_2 molecule, defined as

$$E^{(f)} = \frac{1}{N}\left[E - n_C\varepsilon_g - n_N\varepsilon_{N_2}\right], \tag{1}$$

where N is the number of atoms and E is the total energy of the PCNF, while n_C and n_N are the numbers of C and N atoms, respectively, and ε_g and ε_{N_2} are the total energies per atom of graphene and N_2, respectively. The obtained formation energies are listed in Table 2. As we can see, the $E^{(f)}$ of $C_{60}N_{60}$ is approximately the same as that of C_{60}, while that of $C_{120}N_{60}$ is smaller. Also, that of g-C_2N is smaller than that of g-CN, which is unsurprising as this structure is "closer" to graphene with a larger density of hexagonal rings and a lower percentage of empty space.

5. Thermal stability

Regarding thermal stability, molecular dynamics (MD) simulations were performed utilizing the LAMMPS[45] suite under NVT conditions employing the Nosé–Hoover thermostat,[46,47] for $0 \leq T \leq 2000$ K, with a 100 K increment, and the CHON-2019[48] and GR-RDX-2021[49] ReaxFF potentials. For all calculations, the time step was 0.25 ps. First, an annealing simulation was performed, under NVT conditions, using 2×10^6 time steps, from 300 K down to 0 K, followed by a conjugate gradient optimization to find the energetically optimum structure. Before each NVT simulation at a specific temperature, T, thermalization of the optimized structure at that T was performed, under NVT conditions, for 10^5 time steps, which was

Table 2 Calculated formation energies, $E^{(f)}$, with respect to graphene and N_2 molecule

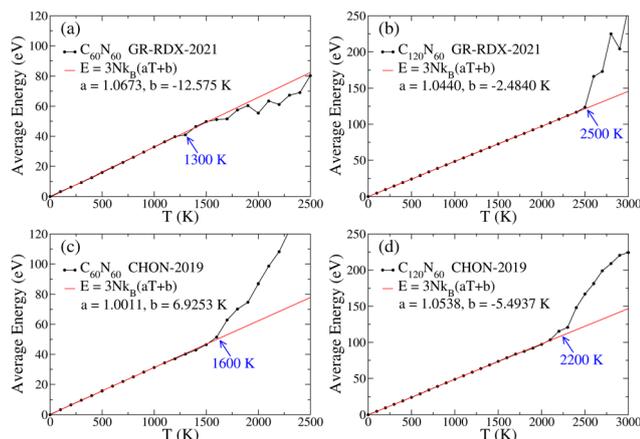|	0D			2D		
	$C_{60}N_{60}$	$C_{120}N_{60}$	C_{60}	g-CN	g-C_2N	Graphene
$E^{(f)}$ (eV)	0.38	0.31	0.38	0.29	0.23	0.00

Fig. 5 Average energy *vs.* temperature obtained from MD simulations using (i) GR-RDX-2021 ReaxFF for $C_{60}N_{60}$ (a) and $C_{120}N_{60}$ (b), and (ii) CHON-2019 ReaxFF for $C_{60}N_{60}$ (c) and $C_{120}N_{60}$ (d). For $C_{60}N_{60}$, $N = 120$, and for $C_{120}N_{60}$, $N = 180$. $k_B = 1/11604.5$ eV K^{-1}. The predicted T_T values are shown in blue.

followed by an MD simulation of 2×10^6 time steps for each temperature, and the time average of the energy, $E(T)$, for each such simulation was calculated.

The obtained $E(T)$ curves are shown in Fig. 5. A divergence in the slope of the Dulong–Petit law ($E = 3Nk_BT$) corresponding to atomic vibrations near the equilibrium positions indicates the initiation of a phase transition (usually accompanied by the coexistence of more phases), which finally leads to the fracture of the molecule. Our estimations of the transition temperature T_T are shown in Fig. 5 with blue, revealing that the T_T values for $C_{60}N_{60}$ and $C_{120}N_{60}$ are well above 1000 and 2000 K, respectively. Similar MD simulations for C_{60} with CHON-2019 predicted that $T_T \gtrsim 3800$ K, which is in agreement with older tight binding MD results,[50] with $3400 < T_T < 3800$ K. While T_T and ν_{min} for $C_{60}N_{60}$ and $C_{120}N_{60}$ are lower than those of C_{60}, they are still sufficiently high, to guarantee that both $C_{60}N_{60}$ and $C_{120}N_{60}$ are thermally stable at temperatures exceeding 1000 K and 2000 K, respectively.

6. On the feasibility of synthesizing $C_{60}N_{60}$ and $C_{120}N_{60}$

Although $C_{60}N_{60}$ and $C_{120}N_{60}$ were found to be extremely stable, the most important issue is their synthesis. Likely, the most promising route involves bottom-up techniques, using proper precursors, similar to the synthesis of g-C_nN_m. Moreover, with appropriate nanosphere precursors containing nitrogen functional groups, nitrogen-doped carbon nanospheres containing pyridinic N atoms have already been synthesized.[51] Additionally, the synthesis of carbon nanospheres with g-C_3N_4 pores has also been reported,[52,53] as well as the synthesis of spherical carbon nitride nanostructures[54] with diameters ranging between 30 nm and 20 μm. In similar experimental studies, the formation of hollow mesoporous carbon nitride microspheres has also been reported.[55] Therefore, the reported

synthesis of both 2D g-C_nN_m membranes[4,8,19,56,57] and carbon nanospheres[58,59] as well as the minimal difference in the calculated formation energies of PCNFs compared to those of their 2D counterparts provide strong evidence for the feasibility of PCNF synthesis.

7. Conclusions

In conclusion, we design and present a novel family of structures, porous carbon nitride fullerenes, representing the 0D analog of 2D porous carbon nitrides, just as fullerenes can be seen as the 0D counterparts of graphene. Our study focuses on the first members of that family of structures with icosahedral symmetry (namely $C_{60}N_{60}$ and $C_{120}N_{60}$), which are derived from the $(n, 0)$ and (n, n) Goldberg polyhedra, respectively, following the two C_N icosahedral fullerene subfamilies with $N = 20n^2$ (C_{20} subfamily) and $N = 60n^2$ (C_{60} subfamily), $n = 1, 2, 3, \ldots$, respectively. We describe, in detail, the design process, for conceptualizing PCNFs, noting that it does not constitute a synthetic route.

Performing DFT calculations with two state-of-the-art functionals (ωB97X-D and MN15), we determined the optimal geometrical properties, the HOMO and LUMO energies, the vibrational frequencies, and the IPs and EAs of $C_{60}N_{60}$ and $C_{120}N_{60}$. Our results reveal that these structures are dynamically stable, while the large values of Δ_{H-L} and η indicate a robust electronic state. Due to their large EAs, these molecules could be used as electron acceptors. Moreover, performing molecular dynamics simulations under NVT conditions, with the CHON-2019 and GR-RDX-2021 ReaxFFs, we showed that $C_{60}N_{60}$ and $C_{120}N_{60}$ PCNFs are thermally stable well above 1000 K and 2000 K, respectively. The pore diameter ($D \approx 4.56$ Å) of their 12 identical N-terminated pentagonal-like pores falls within the range of interest for the permeation of small molecules. Metallic atoms could also be captured in the pore edges for catalytic applications. The unique features of the pentagon-like pores and the particular features arising from the cage shape of these molecules make them potentially interesting for several applications well beyond their 2D counterparts. Therefore, we anticipate that the proposed novel molecules will have a pronounced impact, especially after their synthesis, opening up new directions in research and applications.

Author contributions

ZGF: conceptualization, data curation, formal analysis, investigation, methodology, project administration, resources, software, validation, visualization, writing – original draft, and writing – review and editing. NNL: conceptualization, data curation, formal analysis, investigation, methodology, project administration, resources, software, validation, visualization, writing – original draft, and writing – review and editing.

Data availability

Data for this article are publicly available on Zenodo at **https://doi.org/10.5281/zenodo.14621734**.

Conflicts of interest

There are no conflicts to declare.

Acknowledgements

References

1 H. Montigaud, B. Tanguy, G. Demazeau, I. Alves and S. Courjault, *J. Mater. Sci.*, 2000, **35**, 2547–2552.

2 X. Wang, K. Maeda, X. Chen, K. Takanabe, K. Domen, Y. Hou, X. Fu and M. Antonietti, *J. Am. Chem. Soc.*, 2009, **131**, 1680–1681.

3 P. Kumar, E. Vahidzadeh, U. K. Thakur, P. Kar, K. M. Alam, A. Goswami, N. Mahdi, K. Cui, G. M. Bernard, V. K. Michaelis and K. Shankar, *J. Am. Chem. Soc.*, 2019, **141**, 5415–5436.

4 L. Tan, C. Nie, Z. Ao, H. Sun, T. An and S. Wang, *J. Mater. Chem. A*, 2021, **9**, 17–33.

5 J. Mahmood, E. K. Lee, M. Jung, D. Shin, I.-Y. Jeon, S.-M. Jung, H.-J. Choi, J.-M. Seo, S.-Y. Bae, S.-D. Sohn, N. Park, J. H. Oh, H.-J. Shin and J.-B. Baek, *Nat. Commun.*, 2015, **6**, 6486.

6 S. S. Shinde, C. H. Lee, J.-Y. Yu, D.-H. Kim, S. U. Lee and J.-H. Lee, *ACS Nano*, 2018, **12**, 596–608.

7 N. Fechler, N. P. Zussblatt, R. Rothe, R. Schlögl, M.-G. Willinger, B. F. Chmelka and M. Antonietti, *Adv. Mater.*, 2016, **28**, 1287–1294.

8 C. Moreira Da Silva, M. Vallet, C. Semion, T. Blin, R. Saint-Martin, J. Leroy, D. Dragoé, F. Brisset, C. Gillet, R. Guillot and V. Huc, *Sci. Rep.*, 2023, **13**, 15423.

9 J. Li, C. Cao, J. Hao, H. Qiu, Y. Xu and H. Zhu, *Diamond Relat. Mater.*, 2006, **15**, 1593–1600.

10 Y. Cao, J. Zhao, X. Zhong, G. Zhuang, S. Deng, Z. Wei, Z. Yao and J. Wang, *Green Energy Environ.*, 2021, **6**, 846–857.

11 X. Liu and L. Sheng, *New J. Chem.*, 2022, **46**, 9250–9257.

12 B. L. He, J. S. Shen and Z. X. Tian, *Phys. Chem. Chem. Phys.*, 2016, **18**, 24261–24269.

13 Q. Han, N. Chen, J. Zhang and L. Qu, *Mater. Horiz.*, 2017, **4**, 832–850.

14 Y. Cheng, Y. Song and Y. Zhang, *Phys. Chem. Chem. Phys.*, 2020, **22**, 6772–6782.

15 S. Su, J. Ma, Z. Liu, D. Holiharimanana and H. Sun, *Catalysts*, 2023, **13**, 578.

16 M. Ashwin Kishore, A. O. Sjåstad and P. Ravindran, *Carbon*, 2019, **141**, 50–58.

17 H. Wang, X. Li and J. Yang, *ChemPhysChem*, 2016, **17**, 2100–2104.

18 M. R. Ashwin Kishore and P. Ravindran, *J. Phys. Chem. C*, 2017, **121**, 22216–22224.

19 G. F. S. R. Rocha, M. A. R. da Silva, A. Rogolino, G. A. A. Diab, L. F. G. Noleto, M. Antonietti and I. F. Teixeira, *Chem. Soc. Rev.*, 2023, **52**, 4878–4932.

20 Y.-C. Rao, Z.-Q. Chu, X. Gu and X.-M. Duan, *Comput. Mater. Sci.*, 2019, **161**, 53–57.

21 Y. Qu, F. Li, H. Zhou and M. Zhao, *Sci. Rep.*, 2016, **6**, 19952.

22 Y. Qu, F. Li and M. Zhao, *Sci. Rep.*, 2017, **7**, 1483.

23 Z. Chen, P. Li and C. Wu, *RSC Adv.*, 2015, **5**, 11791–11796.

24 L. Zhu, Q. Xue, X. Li, T. Wu, Y. Jin and W. Xing, *J. Mater. Chem. A*, 2015, **3**, 21351–21356.

25 X. Chang, L. Zhu, Q. Xue, X. Li, T. Guo, X. Li and M. Ma, *J. CO2 Util.*, 2018, **26**, 294–301.

26 X. Wei, Z. Liu, Q. Hou, X. Zhang, Z. Wang, R. Zhang, Y. Yong, H. Cui and X. Li, *J. Ind. Eng. Chem.*, 2024, **131**, 329–336.

27 Y.-s Yu, R.-r Tan and H.-m Ding, *Phys. Chem. Chem. Phys.*, 2020, **22**, 16855–16861.

28 M. Mehrdad and A. Moosavi, *Nanotechnology*, 2020, **32**, 045706.

29 P. Panigrahi, M. Desai, M. K. Talari, H. Bae, H. Lee, R. Ahuja and T. Hussain, *Int. J. Hydrogen Energy*, 2021, **46**, 7371–7380.

30 J. Xu, J. Mahmood, Y. Dou, S. Dou, F. Li, L. Dai and J.-B. Baek, *Adv. Mater.*, 2017, **29**, 1702007.

31 M. Goldberg, *Tohoku Math. J., First Series*, 1937, **43**, 104–108.

32 R. B. King and M. V. Diudea, *J. Math. Chem.*, 2006, **39**, 597–604.

33 J.-D. Chai and M. Head-Gordon, *Phys. Chem. Chem. Phys.*, 2008, **10**, 6615–6620.

34 H. S. Yu, X. He, S. L. Li and D. G. Truhlar, *Chem. Sci.*, 2016, **7**, 5032–5051.

35 M. J. Frisch, G. W. Trucks, H. B. Schlegel, G. E. Scuseria, M. A. Robb, J. R. Cheeseman, G. Scalmani, V. Barone, G. A. Petersson, H. Nakatsuji, X. Li, M. Caricato, A. V. Marenich, J. Bloino, B. G. Janesko, R. Gomperts, B. Mennucci, H. P. Hratchian, J. V. Ortiz, A. F. Izmaylov, J. L. Sonnenberg, D. Williams-Young, F. Ding, F. Lipparini, F. Egidi, J. Goings, B. Peng, A. Petrone, T. Henderson, D. Ranasinghe, V. G. Zakrzewski, J. Gao, N. Rega, G. Zheng, W. Liang, M. Hada, M. Ehara, K. Toyota, R. Fukuda, J. Hasegawa, M. Ishida, T. Nakajima, Y. Honda, O. Kitao, H. Nakai, T. Vreven, K. Throssell, J. A. Montgomery, Jr., J. E. Peralta, F. Ogliaro, M. J. Bearpark, J. J. Heyd, E. N. Brothers, K. N. Kudin, V. N. Staroverov, T. A. Keith, R. Kobayashi, J. Normand, K. Raghavachari, A. P. Rendell, J. C. Burant, S. S. Iyengar, J. Tomasi, M. Cossi, J. M. Millam, M. Klene, C. Adamo,

R. Cammi, J. W. Ochterski, R. L. Martin, K. Morokuma, O. Farkas, J. B. Foresman and D. J. Fox, *Gaussian 16, Revision B.01*, Gaussian Inc., Wallingford CT, 2016.

36 Z. G. Fthenakis, *Carbon*, 2022, **199**, 508–519.

37 Z. G. Fthenakis, *Nanomaterials*, 2023, **13**, 2343.

38 Z. G. Fthenakis, I. D. Petsalakis and N. N. Lathiotakis, *J. Membr. Sci.*, 2025, **713**, 123329.

39 M. E. Foster and B. M. Wong, *J. Chem. Theory Comput.*, 2012, **8**, 2682–2687.

40 Z. C. Wong, W. Y. Fan, T. S. Chwee and M. B. Sullivan, *Phys. Chem. Chem. Phys.*, 2017, **19**, 21046–21057.

41 L. N. Anderson, M. B. Oviedo and B. M. Wong, *J. Chem. Theory Comput.*, 2017, **13**, 1656–1666.

42 Y.-W. Son, M. L. Cohen and S. G. Louie, *Phys. Rev. Lett.*, 2006, **97**, 216803.

43 S. Grimme, J. Antony, S. Ehrlich and H. Krieg, *J. Chem. Phys.*, 2010, **132**, 154104.

44 P. Giannozzi, O. Andreussi, T. Brumme, O. Bunau, M. B. Nardelli, M. Calandra, R. Car, C. Cavazzoni, D. Ceresoli, M. Cococcioni, N. Colonna, I. Carnimeo, A. D. Corso, S. de Gironcoli, P. Delugas, R. A. DiStasio, A. Ferretti, A. Floris, G. Fratesi, G. Fugallo, R. Gebauer, U. Gerstmann, F. Giustino, T. Gorni, J. Jia, M. Kawamura, H.-Y. Ko, A. Kokalj, E. Küçükbenli, M. Lazzeri, M. Marsili, N. Marzari, F. Mauri, N. L. Nguyen, H.-V. Nguyen, A. O. de-la Roza, L. Paulatto, S. Poncé, D. Rocca, R. Sabatini, B. Santra, M. Schlipf, A. P. Seitsonen, A. Smogunov, I. Timrov, T. Thonhauser, P. Umari, N. Vast, X. Wu and S. Baroni, *J. Phys.: Condens. Matter*, 2017, **29**, 465901.

45 A. P. Thompson, H. M. Aktulga, R. Berger, D. S. Bolintineanu, W. M. Brown, P. S. Crozier, P. J. in 't Veld, A. Kohlmeyer, S. G. Moore, T. D. Nguyen, R. Shan, M. J. Stevens, J. Tranchida, C. Trott and S. J. Plimpton, *Comput. Phys. Commun.*, 2022, **271**, 108171.

46 S. Nosé, *J. Chem. Phys.*, 1984, **81**, 511–519.

47 W. G. Hoover, *Phys. Rev. A: At., Mol., Opt. Phys.*, 1985, **31**, 1695–1697.

48 M. Kowalik, C. Ashraf, B. Damirchi, D. Akbarian, S. Rajabpour and A. C. T. van Duin, *J. Phys. Chem. B*, 2019, **123**, 5357–5367.

49 Z. G. Fthenakis, I. D. Petsalakis, V. Tozzini and N. N. Lathiotakis, *Front. Chem.*, 2022, **10**, 951261.

50 S. G. Kim and D. Tománek, *Phys. Rev. Lett.*, 1994, **72**, 2418–2421.

51 H. Zhang, J. Hu, Y. Liu, C. Lin, X. Zhang and Y. Zhang, *ACS Appl. Nano Mater.*, 2023, **6**, 22956–22967.

52 Q. Song, J. Li, L. Wang, L. Pang and H. Liu, *Inorg. Chem.*, 2019, **58**, 10802–10811.

53 Y. Tang, X. Wang, J. Chen, X. Wang, D. Wang and Z. Mao, *Carbon*, 2020, **168**, 458–467.

54 J. L. Zimmerman, R. Williams, V. N. Khabashesku and J. L. Margrave, *Nano Lett.*, 2001, **1**, 731–734.

55 J. Li, L. Han, X. Ye, M. Zhang, Y. Hu and T. Jiang, *Particuology*, 2020, **53**, 186–191.

56 T. S. Miller, A. B. Jorge, T. M. Suter, A. Sella, F. Corà and P. F. McMillan, *Phys. Chem. Chem. Phys.*, 2017, **19**, 15613–15638.

57 C.-Y. Wang, K. Maeda, L.-L. Chang, K.-L. Tung and C. Hu, *Carbon*, 2022, **188**, 482–491.

58 J. Liu, S. Z. Qiao, H. Liu, J. Chen, A. Orpe, D. Zhao and G. Q. M. Lu, *Angew. Chem., Int. Ed.*, 2011, **50**, 5947–5951.

59 Z.-G. Liu, X.-X. He, J.-H. Zhao, C.-M. Xu, Y. Qiao, L. Li and S.-L. Chou, *Chem. Commun.*, 2023, **59**, 4257–4273.